Towards a non-relativistic holographic superfluid

2011 New J. Phys. 13 115008

(http://iopscience.iop.org/1367-2630/13/11/115008)

New Journal of Physics
The open-access journal for physics

Towards a non-relativistic holographic superfluid

Allan Adams[1] **and Juven Wang**
Center for Theoretical Physics, Massachusetts Institute of Technology, Cambridge, MA 02139, USA
E-mail: awa@mit.edu

New Journal of Physics **13** (2011) 115008 (19pp)
Received 5 May 2011
Published 21 November 2011
Online at http://www.njp.org/
doi:10.1088/1367-2630/13/11/115008

Abstract. We explore the phase structure of a holographic toy model of superfluid states in non-relativistic conformal field theories. At low background mass density, we found a familiar second-order transition to a superfluid phase at finite temperature. Increasing the chemical potential for the probe charge density drives this transition strongly first order as the low-temperature superfluid phase merges with a thermodynamically disfavored high-temperature condensed phase. At high background mass density, the system re-enters the normal phase as the temperature is lowered further, hinting at a zero-temperature quantum phase transition as the background density is varied. Given the unusual thermodynamics of the background black hole, however, it seems likely that the true ground state is another configuration altogether.

[1] Author to whom any correspondence should be addressed.

Contents

1. Introduction

Non-relativistic (NR) superfluids provide a high-precision laboratory in which to probe many-body physics in the extreme quantum regime ([1] and references therein). In an effort to bring the tools of holography [2–4] to bear on these systems, considerable effort has been devoted to studying NR deformations of relativistic examples[2] which enjoy $z = 2$ scaling [7–11]. Unfortunately, such deformations generate highly atypical states in the resulting NRCFT whose thermodynamic and other properties are tightly constrained by their relativistic births. In particular, they are in general far from the superfluid ground states of the corresponding systems, for which we currently have no description.

In this paper, we examine certain superfluid states in a holographic NRCFT in a probe approximation. Our strategy is essentially the same as that in the AdS case (see e.g. [12, 13]): we study an Abelian–Higgs theory in the background of a neutral asymptotically Schrödinger black hole [9–11] in the probe approximation. Several features of the geometry, however, make the resulting analysis qualitatively different. For example, we are now forced to turn on two components of the bulk gauge field: A_t, dual to a boundary charge current, and A_ξ, dual to a boundary mass[3] current. By itself, this is not a big deal. What is surprising

[2] Since the NR conformal group is a subgroup of the relativistic group in one higher dimension, we can construct a non-relativistic conformal field theory (NRCFT) by turning on an operator in a relativistic conformal field theory (CFT) which breaks the relativistic group to its NR subgroup. Taking the operator to be marginal in the NRCFT [5, 6] requires it to be irrelevant in the CFT. Holographically, this corresponds to a one-parameter deformation of the geometry which alters the asymptotic geometry from anti-de Sitter (AdS), whose isometries form the relativistic conformal group, to Schrödinger [7, 8], whose isometries fill out the NR conformal group.

[3] In an NRCFT, each primary operator is characterized not only by a dimension Δ but also by its mass, M, where mass is the name of a central extension $\hat{M}$ in the NR conformal group. In the case of free fermions, $\hat{M} = M\psi^\dagger\psi$; hence, it is often called the 'number' operator—we prefer 'mass' to disambiguate the various meanings of 'number'.

given intuition from the relativistic case is that the boundary value of this second vector component, $M_o = A_\xi|_\partial$, weasels its way into the *dimension* of the boundary order parameter as $\Delta = 2 \pm \sqrt{4 + m^2 + q^2 M_o^2}$. Specifying the boundary NRCFT thus requires specifying not just the bulk matter fields and their interactions, but also the asymptotic fall-offs of some of the bulk fields. Similar effects arise in the holographic renormalization of the theory, which as usual requires introducing counterterms that depend on the boundary operator dimensions; here, these counterterms will depend explicitly on the boundary values of some bulk fields, too (see e.g. [14] for a discussion of such effects).

To build a truly NR superfluid then, we must generate a condensate for a boundary operator with non-zero mass eigenvalue, $M \neq 0$. This is the role of the second component of the gauge field—in a gauge where the phase of the condensate is constant, the mass eigenvalue is simply $M = -q\, M_o$. The boundary value of the second component of the gauge field thus controls the breaking of the mass symmetry in the superfluid phase.

While the background about which we perturb is a one-parameter deformation of a relativistic example, the superfluid state we find is not, and indeed enjoys quite distinct phenomenology from its AdS cousins. Fundamentally, the NR condensate is characterized by one more quantum number than in the relativistic case—the mass eigenvalue, M, of the order parameter—with the NR condensate breaking the symmetry generated by the mass operator, a key signature of an NR superfluid. As we shall see, this leads to a host of interesting effects in the strongly NR regime, including the appearance of a thermodynamically unstable high-temperature condensed phase that drives the superconducting transition from second order to first at a multicritical point, the persistence of a condensate even in the absence of a chemical potential for the charge density, and re-entrance of the normal phase at low temperatures for a sufficiently large background density.

It is tempting to interpret this re-entrance as signaling a zero-temperature quantum phase transition as the background mass density is tuned. However, the re-entrant normal state is again the simple one-parameter deformation which we do not expect to be the true equilibrium ground state, so we do not expect this probe analysis to be the end of the story. Meanwhile, it remains possible that the system is in fact re-entrant for all values of the background mass density as $T \to 0$, where our probe approximation becomes unreliable. Resolving these puzzles, however, requires going beyond the truncated probe approximation discussed in this paper; we leave them to a future study.

The plan of this paper is as follows. In section 2, we quickly describe the basic strategy and computational setup, with various details elaborated in the appendices. In section 3, we explore the phenomenology and phase structure of holographic superfluids outside a Schrödinger black hole (an analogous study in the background of a Schrödinger soliton [15] is performed in appendix A—while this is not in the same ensemble as the black hole, it provides an alternate example with surprising physics of its own). We end the paper in section 5 with a summary and list of next steps.

2. The setup

Our basic strategy involves studying an Abelian–Higgs system,

$$\mathcal{L}_{\text{probe}} = \frac{1}{e^2}\left(-\frac{1}{4}F^2 - |\mathcal{D}\Phi|^2 - m^2|\Phi|^2\right), \tag{2.1}$$

as a perturbation around the planar Schrödinger black-hole background,

$$ds^2 = \left(-f + \frac{(f-1)^2}{4(K-1)}\right)\frac{dt^2}{Kr^4} + \frac{1+f}{r^2 K}dt\,d\xi + \frac{K-1}{K}d\xi^2 + \frac{d\vec{x}^2}{r^2} + \frac{dr^2}{fr^2} \tag{2.2}$$

in the probe limit $e^2 \to \infty$. Here, $f = 1 - r^4(\pi T\Omega)^{4/3}$, $K = 1 + r^2\Omega^2$ and the metric is given in string frame. One can think of this as a rather extreme truncation of the charged Schrödinger black-hole system [16, 17] where we drop the coupling of the vector to the scalar and massive vector of the black-hole background, or simply as a holographic toy model. The geometry is controlled by two physical parameters, the background mass density, Ω, and the temperature, T, with the horizon located at the radial coordinate $r_H = (\pi T\Omega)^{-1/3}$.

For spatially homogeneous solutions, we can without loss of generality set $\vec{A} = 0$ and take $\Phi = \phi(r)$ and $A = A_t(r)dt + A_\xi(r)d\xi$. In the Einstein frame, the equations of motion take the form

$$f^2 r^2\phi'' - f(4-f)r\phi' - \Bigg[f\left(q^2A_\xi^2 + 2q^2r^2A_\xi A_t + m^2K^{1/3}\right) - \frac{q^2(f-1)^2}{4(K-1)}\left(A_\xi - 2r_H^4\Omega^2 A_t\right)^2\Bigg]\phi = 0, \tag{2.3}$$

$$fr^2A_t'' - \left(2 - \frac{f}{3}(7K-4)\right)\frac{r}{K}A_t' - \left(2 + f(f-1) + \frac{(f-1)^2}{K-1}\right)\frac{1}{Kr}A_\xi' - 2q^2K^{1/3}\phi^2A_t = 0, \tag{2.4}$$

$$fr^2A_\xi'' - \left(4K - 2 - \frac{2+K}{3}f\right)\frac{r}{K}A_\xi' - 4(K-1)\frac{r^3}{K}A_t' - 2q^2K^{1/3}\phi^2A_\xi = 0. \tag{2.5}$$

Note that $A_\xi \neq A_t$.

2.1. Asymptotic behavior and the holographic dictionary

Near the boundary at $r = 0$, the vector components behave as

$$A_t = \mu_Q + \rho_Q r^2 + \cdots, \quad A_\xi = M_o + \rho_M r^2 + \cdots, \tag{2.6}$$

where the various $\cdots$ represent various (possibly non-normalizable) terms whose coefficients are entirely fixed by the equations of motion and the values of these integration constants, μ_Q, ρ_Q, M_o and ρ_M.[4] As usual, μ_Q represents the chemical potential per unit charge, which

[4] In particular, the leading term for A_t runs as $-2\rho_M\log(r)$. While formally the dominant term, it is determined by the equations of motion and ρ_M and thus does not represent an independent mode of the system. Importantly, due to factors of the inverse metric, this log running does not lead any components of the bulk stress tensor to diverge. A complete holographic renormalization of this system would settle the dictionary, but is beyond the scope of this paper; for the moment we simply take the above dictionary as a provisional interpretation which is supported by the consistency of the results below. Interestingly, while A_t has no log in fully backreacted charged-black-hole solutions [16, 17], linearizing the Maxwell equation around these solutions does generate a log without changing any other of the asymptotics of the vector, so this log is likely a simple consequence of an extreme truncation of the full charged-black-hole system. It would be interesting to study the full system and see what, if anything, changes.

effectively sets the zero of energy in the boundary theory—the gauge-invariant bulk quantity that becomes the boundary Hamiltonian acting on the operator dual to the bulk matter field of charge q is $(\mathrm{i}\partial_t + qA_t)$; at the boundary, for plane waves $\mathrm{e}^{-\mathrm{i}\omega t}$, this becomes $(\omega + q\mu_Q)$. Thus, one insertion of the charged operator $\mathcal{O}\,\mathrm{e}^{-\mathrm{i}\omega t}$ costs $\delta E = (\omega + q\mu_Q)$. As usual, ρ_Q computes the induced charge density.

It might be tempting to think of M_o as a chemical potential for the mass operator, $\hat{M}$. However, this is not quite right—it is a superselection parameter. Recall that, holographically,

$$\hat{M} \equiv \hat{P}_\xi|_\partial = -\mathrm{i}(\partial_\xi - \mathrm{i}qA_\xi)|_\partial, \tag{2.7}$$

i.e. $\hat{M}$ is the boundary value of the gauge-invariant ξ-momentum in the bulk. The mass eigenvalue of a boundary operator dual to a bulk field with ξ-momentum ℓ and charge q is thus $M = (\ell - qM_\mathrm{o})$, where $M_\mathrm{o} = A_\xi|_\partial$. Like a chemical potential, M_o sets a bias for the mass M, shifting it away from its ξ-momentum, ℓ. But the mass in an NRCFT is not a parameter; it is part of the definition of the theory. Thus, once we fix gauge in the bulk, different values of $A_\xi|_\partial$ correspond to distinct NRCFTs, not to a fixed theory with different background fields turned on. In particular, as we will see momentarily, the dimensions of various boundary operators depend on $A_\xi|_\partial$, an unfamiliar effect. ρ_M computes the mass density coupled to A_μ. Henceforth, we fix gauge in the bulk such that $\ell = 0$ and $M = -qA_\xi|_\partial$.

As for our charged scalar, near the boundary at $r \to 0$ it behaves as

$$\phi \sim \phi_1 r^{\Delta_-} + \phi_2 r^{\Delta_+} + \cdots, \tag{2.8}$$

where

$$\Delta_\pm = 2 \pm \sqrt{4 + m^2 + q^2 M_\mathrm{o}^2}\,. \tag{2.9}$$

(Note that we will occasionally write Δ_1 and Δ_2 for Δ_- and Δ_+, respectively.) In the window $1 < \Delta_- < 2$, both components $\phi_{1,2}$ are normalizable, so we may interpret either of $\phi_{1,2}$ as the vev $\langle\mathcal{O}\rangle$, with the other representing the source $\mathcal{J}$. These two choices correspond to alternate quantizations of the boundary NRCFT [7, 18] encoding inequivalent physics. The 'standard' quantization fixes $\phi_1 \propto \mathcal{J}$ as the source with $\phi_2 \propto \langle\mathcal{O}\rangle$ the response. We will mostly focus on the 'alternate' quantization with $\mathcal{J} \propto \phi_2$ and $\langle\mathcal{O}\rangle \propto \phi_1$ for reasons that will become clear in the next section.

Importantly, the dimensions, $\Delta_\pm$, depend not only on the mass of the bulk scalar, as in AdS, but also on the boundary value of a bulk field, $M_\mathrm{o} = A_\xi|_\partial$. As discussed above, by the holographic relation $\hat{M} \equiv -\mathrm{i}(\partial_\xi - \mathrm{i}qA_\xi)|_\partial$, this quantity is nothing but the mass eigenvalue of the dual operator,

$$M = -qA_\xi|_\partial = -qM_\mathrm{o}.$$

Our expression for the dimensions above then becomes $\Delta_\pm = 2 \pm \sqrt{4 + m^2 + M^2}$, which is the expected form [7, 8], including the quadratic dependence on M inside the radical.

Now, as discussed in [9–11], the free energy of the full system takes the form $F \equiv E + \mu_M \hat{M}$, where $\mu_M = \frac{-1}{2\Omega^2 r_\mathrm{H}^4}$ is determined by the background spacetime. The total free energy per insertion of an operator dual to a bulk field with ξ-momentum ℓ, frequency ω, and coupled with charge q to our gauge field is thus $\delta F = (\omega + q\mu_Q) + \mu_M M$, where $M = (\ell - qM_\mathrm{o})$.

2.2. Near-horizon behavior and setting up the calculation

In the bulk, we are thus left with a six-parameter family of solutions labeled by sources (μ_Q, M_o, $\mathcal{J}$) and responses (ρ_Q, ρ_M, $\langle\mathcal{O}\rangle$). Holographically, we expect boundary conditions at the horizon, where the radial equations of motion degenerate, to impose three additional constraints. Together with the two parameters T and Ω of the background geometry, this should leave us with a five-parameter phase space. To verify this, we need to study the behavior of our solutions near the horizon.

The equations of motion degenerate at the black-hole horizon, so we must impose boundary conditions to pick the appropriate solutions. As usual, it suffices to impose regularity at the horizon, which is in any case necessary for the validity of the probe approximation. Assuming regularity, the equations of motion as presented in (2.3)–(2.5) degenerate into three algebraic equations relating the six horizon values of the fields and their derivatives, as expected,

$$\left(A_\xi(r_H) - 2r_H^4\Omega^2 A_t(r_H)\right)^2 \phi(r_H) = 0, \tag{2.10}$$

$$-2r_H^2 A_t'(r_H) + \left(\frac{2K_H - 1}{K_H - 1}\right) A_\xi'(r_H) + 2q^2 r_H K_H^{4/3}\phi^2(r_H)A_t(r_H) = 0, \tag{2.11}$$

$$4r_H\phi'(r_H) + \left(4K_H(K_H-1)r_H^4 q^2 A_t^2(r_H) + m^2 K^{1/3}\right)\phi(r_H) = 0. \tag{2.12}$$

This suggests a simple numerical strategy for constructing superfluid states of our holographic NRCFT. To specify a solution to the full equations of motion, we fix any three of μ_Q, M_o, $\mathcal{J}$, ρ_Q, ρ_M and $\langle\mathcal{O}\rangle$ at the boundary and impose the above regularity conditions at the horizon. Since we are interested in spontaneously generated condensates, we will generally set $\mathcal{J} = 0$. The resulting two-point boundary value problem can be solved numerically in various ways. The most straightforward is a brute-force shooting method, as typically employed in the relativistic case.

In sweeping out parameter space, however, we must be careful to vary the *parameters* of the NRCFT while holding the NRCFT itself fixed—i.e. while holding the spectrum of quantum numbers fixed. This is straightforward in AdS, where fixing the set of dimensions reduces to fixing the bulk mass m^2 of the bulk scalar. Here, however, the dimension Δ and mass M of the boundary scalar operator depend on the asymptotic value of A_ξ as $M = -qA_\xi|_\partial$ and $\Delta_\pm = 2 \pm \sqrt{4 + m^2 + M^2}$. Before sweeping out parameter space, then, we must fix $A_\xi|_\partial = M_o$. As we have already set $\mathcal{J} = 0$, fixing the system thus leaves us with a three-parameter phase space labeled by μ_Q, Ω and T.

This peculiar behavior—that the definition of the boundary CFT depends on the boundary behavior of the bulk fields—is a very general phenomenon in the Schrödinger holography. Indeed, renormalizing the boundary stress tensor, say, or other operators in the boundary NRCFT requires counterterms which are local in time and space, but which depend explicitly on dimensions, Δ, and thus on the asymptotic values of A_ξ, in a mildly non-local fashion. Such field-dependent counterterms have appeared previously in attempts to renormalize holographic NRCFTs, most recently in [14]. A complete understanding of the holographic renormalization of these theories is clearly of considerable interest.

2.3. Conductivity

We can compute the conductivity in our superconducting background by studying the linear response to a time-dependent vector potential $A_x \sim \mathrm{e}^{-\mathrm{i}\omega t}$. As usual, this boils down to solving the equation of motion for the bulk gauge component A_x linearized about the superfluid background and subject to infalling boundary conditions at the horizon. Setting $A_x = a(x)\,\mathrm{e}^{-\mathrm{i}\omega t}$, we have

$$f r^2 a_x'' - \left(4 - f\frac{2+7K}{3K}\right) r a_x' + \left(\frac{\omega^2 r^4 (K-1)}{f} - 2q^2 K^{1/3}\phi^2\right) a_x = 0. \tag{2.13}$$

Near the horizon, this reduces to

$$\left(\omega^2 + \left(\frac{4\epsilon}{r_{\mathrm{H}}^3 \Omega}\frac{\mathrm{d}}{\mathrm{d}\epsilon}\right)^2\right) a_x(\epsilon) \simeq 0, \tag{2.14}$$

where $r = r_{\mathrm{H}} - \epsilon$. The infalling solutions thus take the form

$$A_x = a_0\,\mathrm{e}^{-\mathrm{i}\omega t}(r - r_{\mathrm{H}})^{-\mathrm{i}\omega/4\pi T}(1 + a_1(r - r_{\mathrm{H}}) + \cdots). \tag{2.15}$$

Near the boundary,

$$A_x = A_0 + A_2\frac{r^2}{2} + \cdots.$$

A short computation then verifies that the conductivity is given by

$$\sigma(\omega) = \frac{\langle J_x\rangle}{\langle E_x\rangle} = -\mathrm{i}\frac{\langle J_x\rangle}{\omega\langle A_x\rangle} = -\mathrm{i}\frac{A_2}{\omega A_0}.$$

Note that since we are solving a linear equation but only care about this ratio, the overall scale of A_x is immaterial. We can use this freedom to set $a_0 = 1$, which simplifies the numerical problem.

Notably, we can analytically determine the ω-dependence of σ for large and small ω via standard power-series analysis. The scaling superfluid turns out to be independent of Δ and M. At small frequency, we find that

$$\mathrm{Im}[\sigma(\omega \ll 1)] \propto \omega^{-1}, \tag{2.16}$$

whereas for large ω, we have

$$\mathrm{Re}[\sigma(\omega \gg 1)] \propto \omega^{-1/3} \qquad \mathrm{Im}[\sigma(\omega \gg 1)] \propto \omega^{-1/3}. \tag{2.17}$$

This last result unsurprisingly differs from the AdS case, where $\mathrm{Re}[\sigma(\omega \gg 1)] = 1$. Reassuringly, they both match the numerical results presented below, a nice sanity check.

3. Phases of a Schrödinger superfluid

Thus armed, we now get down to the business of finding a superfluid state in our NR holographic CFT and exploring its phase diagram. *A priori*, the phase space is fairly high-dimensional—specifying a point involves fixing Δ and M to fix the theory, then tuning μ_Q, T and Ω to sweep out the phase diagram. For simplicity, we will begin by picking convenient values $\Delta = 6/5$, $M = 1/2$ and $\mu_Q = 1/8$ and then dial the background mass density, Ω. This will reveal a zero-temperature quantum phase transition at a critical value Ω_*. We will then fix Ω and vary μ_Q, which will drive the superconducting phase transition from the second to first order.

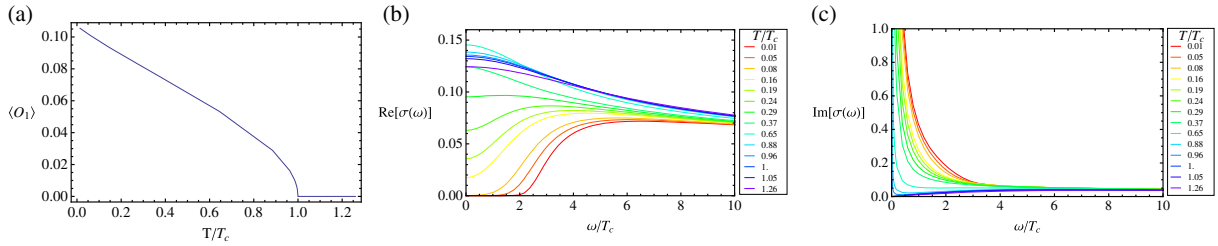

Figure 1. At small Ω, the behavior of the superfluid is essentially the same as that in AdS, with a second-order mean-field phase transition at the onset of superconductivity at T_c, including the familiar gap-and-pole form in the ac conductivity, leaving us in a happy superfluid state at $T = 0$. Here, $(\mu_Q, \Omega) = (1/8, 1/16)$, with $T_C = 0.505$.

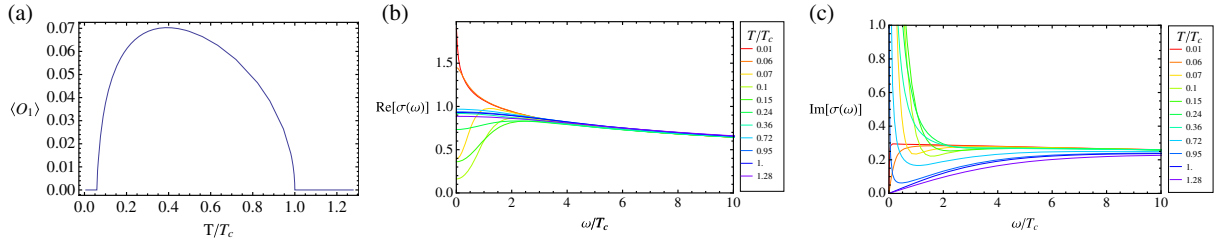

Figure 2. At large Ω, in addition to the original transition to a superconducting state at T_c, the system now exhibits re-entrance of the normal phase at a new low-temperature second-order transition at T_L, again with mean-field exponents. Below T_L, σ behaves like the normal gas. Here $(\mu_Q, \Omega) = (1/8, 1)$ with $T_C = 0.149$ and $T_L = 0.009$.

3.1. Varying Ω and a quantum phase transition?

We begin by fixing $\Delta = 6/5$ and $M = 1/2$, then set $\mu_Q = 1/8$ and vary Ω between 0 and 1. The basic results are presented in figures 1–3, which plot the condensate $\langle \mathcal{O}(T) \rangle$ as a function of temperature, as well as the ac conductivities $\mathrm{Re}[\sigma(\omega)]$ and $\mathrm{Im}[\sigma(\omega)]$, for $\Omega = \frac{1}{16}, \frac{3}{8}$ and 1, respectively. These results are discussed in detail below.

- $\Omega \ll \Omega_*$. For very small Ω, the geometry remains essentially AdS until very close to the boundary, so we expect most low-energy physics—such as superfluid condensation—to very closely track familiar AdS results. This turns out to be almost correct, modulo a surprise we will explore shortly.
  Figure 1(a) shows the condensate as a function of temperature for the alternate quantization ($\langle \mathcal{O} \rangle \sim \phi_1$) for $\Omega = 1/16$. As is clear by eye and can be checked precisely from the numerics, the resulting condensate turns on at $T = T_c$ with classic mean-field behavior ($\beta_c = \frac{1}{2}$) and grows as the temperature is lowered. Figures 1(b) and (c) then show the real and imaginary parts of the ac conductivity for various temperatures indicated by color, from high (violet) to low (red). These demonstrate the appearance of a superconducting state at T_c, with the gap growing as the temperature is lowered. Note, too, that the conductivity

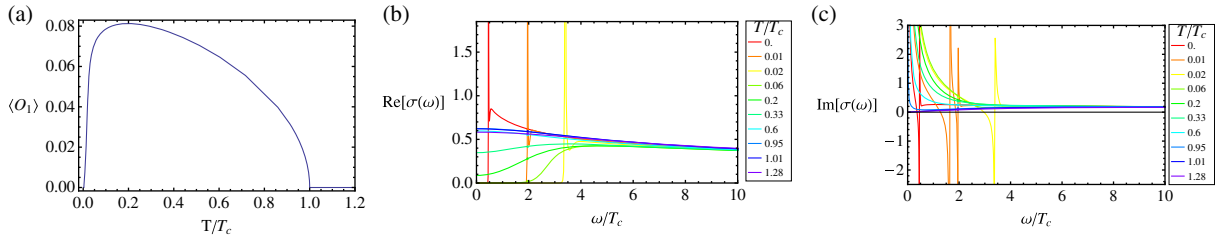

Figure 3. At intermediate Ω, we again have a second-order mean-field transition into a superfluid state at T_c. At low temperatures, however, the system undergoes a non-mean-field transition to an apparently insulating state. Here $(\mu_Q, \Omega) = (1/8, 3/8)$ with $T_C = 0.123$.

in the superfluid phase has $\mathrm{Im}[\sigma(\omega \to 0)] \sim 1/\omega$, while $\mathrm{Re}[\sigma(\omega \to \infty)] \sim \mathrm{Im}[\sigma(\omega \to \infty)] \sim \omega^{-1/3}$. This scaling is expected on general grounds, so gives us confidence in our numerical results.

- $\Omega \gg \Omega_*$. As we increase the background number density, the story changes dramatically. Figure 2 shows the same plots as figure 1 but with $\Omega = 1$ rather than $\Omega = 1/16$. The most obvious difference is that the order parameter *vanishes* at a sufficiently low temperature, $T \leqslant T_L$, doing so again with mean-field behavior. As is clear from the finite value of $\mathrm{Re}[\sigma(0)]$, the extreme low-temperature phase is again metallic.
  Consider now the behavior of the system at zero temperature as a function of the background number density, Ω. As $\Omega \to 0$, the system is superconducting. As $\Omega \to 1$, the metallic phase is re-entrant. At some critical Ω_*, then, the zero-temperature system appears to undergo a superconductor–metal quantum phase transition.
- $\Omega \to \Omega_*$. It is tempting to try to determine what happens as we tune Ω towards this critical Ω_*. Figure 3 shows the same system at Ω slightly above Ω_*.
  As before, there is a phase transition at T_c with standard mean-field behavior. The zero-temperature behavior, however, differs dramatically from mean-field expectations; rather, at low temperature, the condensate decays exponentially, as does the superfluid density, while the normal density remains vanishing and the conductivity heavily suppressed at small but non-vanishing ω, suggesting that the $T = 0$ state is not metallic. It is tempting to read this as indicating a translationally invariant insulating phase.
  However, numerical results in this region should be taken with a sizeable grain of salt. Indeed, at a sufficiently low temperature, the numerics simply fail to converge. More physically, in this regime, the probe approximation is becoming dangerously unreliable—the matter field profiles which generate the required boundary values grow rapidly deep in the bulk (and in particular near the horizon) as we approach $T = 0$ or Ω_*. Backreaction may thus qualitatively alter the low-temperature physics, either near the transition at $\Omega \sim \Omega_*$ or for sufficiently low T at any Ω.
  Indeed, it is entirely possible that the backreacted solution is re-entrant at any value of Ω; our analysis is only reliable sufficiently far away from $T = 0$. To unambiguously exclude re-entrance at small Ω as $T \to 0$ requires including backreaction, which is beyond the scope of this paper. Note, however, that the probe approximation shows no signs of inconsistency for $\Omega > \Omega_*$, so we can be quite confident that the system is definitely re-entrant at sufficiently large Ω.

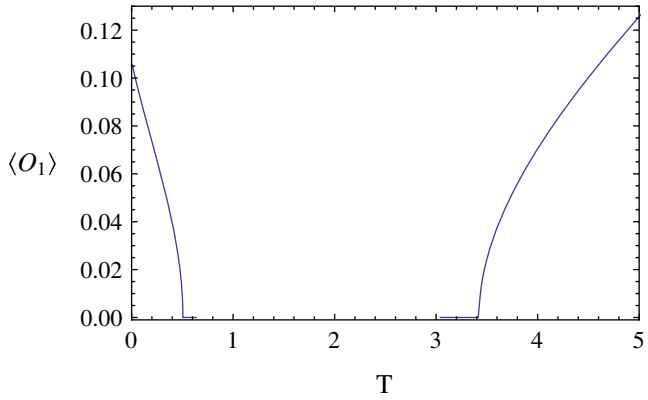

Figure 4. Surprisingly, there is another condensed phase at *high* temperatures. Here $(\mu_Q, \Omega) = (1/8, 1/16)$.

3.2. High-temperature condensates and the free energy

The surprise alluded to above involves the *high*-temperature limit. Figure 4 shows the same system but now extending to higher temperatures. The surprise is the appearance of a *high-temperature* condensate at $T \geqslant T_{\rm H}$. Troublingly, the condensate appears to grow without bound as the temperature increases[5].

Before we panic, however, we should verify that this high-temperature condensate is in fact thermodynamically favored over the trivial vacuum. Holographically, this means we are computing the holographically renormalized on-shell action. Unfortunately, in asymptotically Schrödinger spacetimes, holographically renormalizing the action is exceedingly complicated. Happily, a simple strategy allows us to compute the difference in free energy between condensed and vacuum states without performing a full renormalization of the action[6].

The basic idea goes as follows. Generally, specifying the non-normalizable (source) mode ϕ_1 of the bulk scalar determines the normalizable (response) mode, ϕ_2. Smoothly varying the source thus traces out a curve $\phi_2(\phi_1)$ in the (ϕ_1, ϕ_2) plane. Along this flow, we can ask how the free energy—aka the Euclidean action—varies. Given the properly renormalized action, the variation of the full bulk action takes the form $\delta S_{\rm eff} = \cdots \delta\phi_i + \cdots \delta A_i$ where $\delta\phi_i$ and δA_i are the variations of the bulk fields and the $\cdots$ correspond to the bulk equations of motion. So long as we satisfy the bulk equations of motion, this reduces to a simple boundary term, $\delta S = (\Delta_1 - \Delta_2) \int_{\partial_M} \phi_2\, \delta\phi_1 - 2 \int_{\partial_M} (\rho_M\, \delta\mu_Q + \rho_Q\, \delta M_{\rm o})$. Moreover, if we fix the asymptotic values of A_i (corresponding to fixing the values of the chemical potential $\mu_Q = A_t|_\partial$ and the mass $M = A_\xi|_\partial$), this further simplifies to $\delta S = (\Delta_1 - \Delta_2) \int_{\partial_M} \phi_2\, \delta\phi_1$. We can thus compute the relative free energy density ($\mathcal{F}_A - \mathcal{F}_B$) between any two states A and B connected by such a flow by integrating δS along the flow,

$$\mathcal{F}_B - \mathcal{F}_A = -T \int_A^B \frac{\delta S_E}{V_D} = -T(\Delta_1 - \Delta_2) \int_A^B \phi_2\, {\rm d}\phi_1, \tag{3.1}$$

[5] Such a high-temperature instability was predicted by Cremonesi *et al* [19] whenever $\Delta \leqslant 4$.

[6] We thank Nabil Iqbal for illuminating discussions on this topic; see [20] in which this approach is developed further.

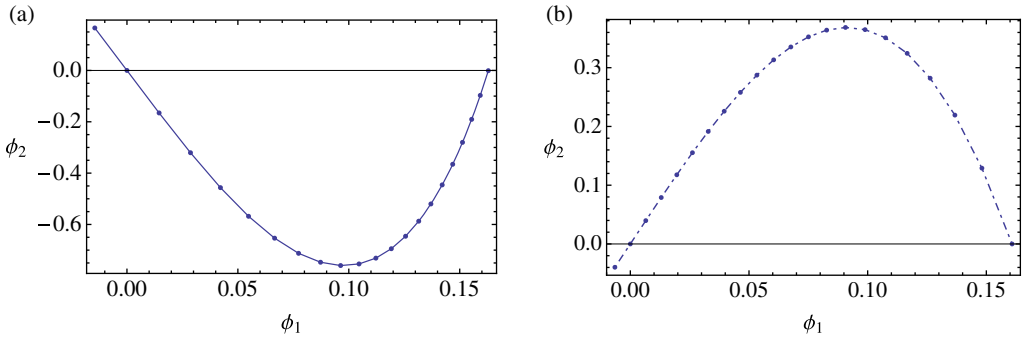

Figure 5. (a) The low-T condensate has smaller free energy than the non-condensed phase, $\mathcal{F}_C - \mathcal{F}_N < 0$. (b) The high-$T$ condensate has larger free energy than the non-condensed phase, $\mathcal{F}_C - \mathcal{F}_N > 0$. One can determine the sign of $\mathcal{F}_C - \mathcal{F}_N$ from the orientation of the curve. Here $(\mu_Q, \Omega) = (3/8, 1/16)$.

where V_D is the volume of the boundary theory and the integral is performed along the flow specified above. By construction, this agrees with what we would get by evaluating the fully holographically renormalized free energy for each solution and subtracting. Happily, this allows us to compute the correct free energy without having to worry about the full holographic renormalization of the theory (for a further comparison of holographic renormalization and our method, see [14, 21, 22]).

Now consider the case of our holographic superfluid in alternate quantization, where $\phi_2 = \mathcal{J}$ is the source and $\phi_1 = \langle \mathcal{O} \rangle$ is the response. In this case, the curve $\phi_1(\phi_2)$ is multivalued over $\phi_2 = 0$, with one solution corresponding to the trivial vacuum, $\langle \mathcal{O} \rangle = 0$, and one to the non-trivial condensate, $\langle \mathcal{O} \rangle \neq 0$. As outlined above, these two solutions are connected by a very specific flow in the (ϕ_1, ϕ_2) plane. To compute the properly renormalized relative free energy, then, all we must do is find this flow and integrate along it,

$$\mathcal{F}_C - \mathcal{F}_N = -T(\Delta_1 - \Delta_2) \int_N^C \phi_2 \, \mathrm{d}\phi_1, \tag{3.2}$$

where the integration is again along the flow defined above. If this difference is negative, the condensate is thermodynamically favored.

Figure 5 plots two such flows. On the left, we have a flow connecting the trivial vacuum ($\phi_1 = \phi_2 = 0$) to a symmetry-breaking vacuum ($\phi_1 \neq 0$, $\phi_2 = 0$) in the alternate quantization in the low-temperature regime, with the flow indicated by the solid line and the direction of flow defining the direction of integration. The area under the curve, corresponding to the free energy of the condensed state, is negative. On the right is the analogous flow in the high-temperature regime—here the free energy is positive. We thus deduce that the low-temperature condensate is thermodynamically stable, while the high-temperature condensate is unstable, in the alternate quantization.

What about the standard quantization? Figure 6(a) plots the condensate in standard quantization as a function of temperature. Note that there is no separate low- versus high-temperature condensate, just a single continuous instability whose profile grows with temperature. Figure 6(b) then shows a typical flow at typical temperature. Importantly, the enclosed area is negative for every temperature, indicating a thermodynamic instability even at

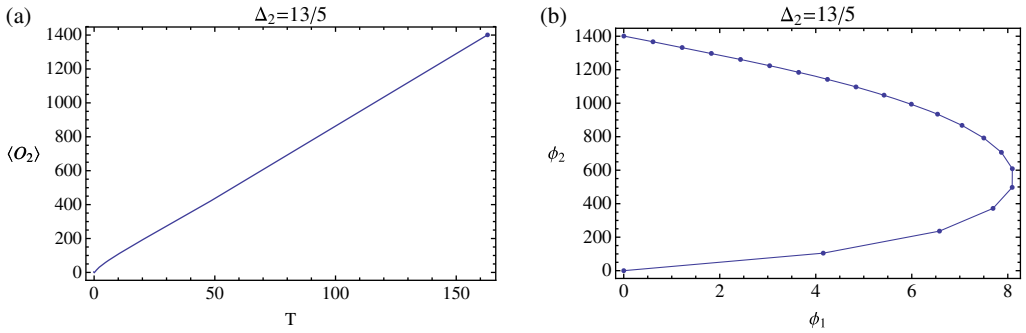

Figure 6. (a) Condensate as a function of T for the standard quantization, with $\Delta_2 = 13/5$. (b) Typical flow at generic temperature, indicating a thermodynamic instability at every temperature.

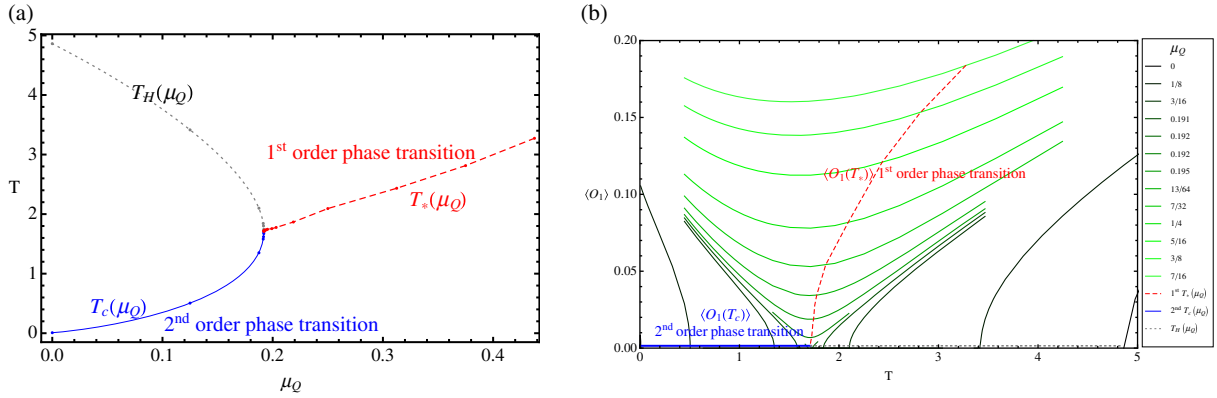

Figure 7. At $\mu_Q > \mu_* \sim 0.192$, the transition goes first order. Here, $\Omega = 1/16$.

arbitrarily high temperature. This is why we quietly chose the alternate quantization in section 2. It would be interesting to understand the meaning of this instability in detail.

3.3. Varying μ_Q and a multicritical point

The thermodynamic instability of the high-temperature condensate leads to an important physical effect as we vary μ_Q. Figure 7(a) plots $T_c(\mu_Q)$ and $T_H(\mu_Q)$, the critical temperatures for the low- and high-temperature condensates as a function of the chemical potential μ_Q. As we crank up μ_Q, holding all other parameters fixed, T_c increases while T_H decreases. At a critical value, μ_*, the two critical points merge; above μ_*, the condensate is non-zero for all temperatures. This is clear from figure 7(b), where we plot the order parameter as a function of temperature for values of the chemical potential above and below this critical μ_*.

However, we have already checked that the condensed phase is thermodynamically disfavored at high temperatures. For $\mu_Q > \mu_*$, then, there must be a critical temperature, T_*, above which the smoothly varying, non-vanishing condensate becomes thermodynamically disfavored. This temperature is indicated by the red dashed curves in figures 7(a) and (b).

We can verify this by computing the relative free energy of the condensed phase as we vary the temperature. Figure 8(a) shows the flows associated with points to the left

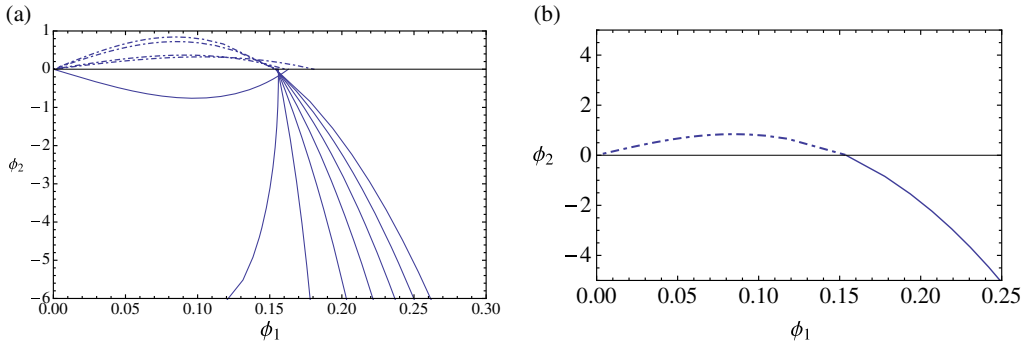

Figure 8. (a) Flow lines in the neighborhood of the critical temperature, for $\mu_Q = 3/8$. (b) The flow switches direction discontinuously (lower solid to upper dashed curves) at a critical temperature T_* indicated by the red dashed curve in figure 7, leading to a first-order phase transition at T_*. Here, $\mu_Q = 3/8$ and $\Omega = 1/16$.

and right of the critical temperature where the low- and high-temperature instabilities meet (indicated by the red dashed curve in figure 7(b)). Figure 8(b) focuses on the immediate neighborhood of the transition temperature for $\mu_Q > \mu_*$. For all temperatures below the critical temperature, the flows go below the horizontal axis, corresponding to a negative free energy and a thermodynamically stable condensate. For all temperatures above the critical temperature, the flows go above the horizontal axis, so the condensate is thermodynamically disfavored at high temperatures. Indeed, while the value of the condensate is non-vanishing and in fact completely smooth as we flow through T_*, the path that carries us from the trivial state to the condensate changes discontinuously as we pass through T_*. As a result, the integrated area—and thus the free energy—also changes discontinuously at T_*. Moreover, as we take $\mu_Q \to \mu_*$, the value of the condensate at the transition goes to zero, $\langle \mathcal{O}(T_*) \rangle \to 0$; this ensures that the latent heat of the transition goes to zero at the multicritical point where the transition switches from first to second order, as expected on general grounds.

The upshot of all of the above is that as we raise μ_Q, the phase transition from high-temperature metal to low-temperature superfluid switches from second order to first, with the transition occurring at a multicritical point where the low- and high-temperature superfluid phases collide. Near the phase transition boundaries, including the multicritical point, the order parameter scales with simple mean-field exponents. More precisely, near the finite temperature second-order phase transition, $\langle \mathcal{O} \rangle \sim (T_c - T)^{1/2}$, while near the first-order phase transition boundary when $\mu_Q > \mu_*$ the condensate jumps discontinuously at T_*, with $\langle \mathcal{O}(T_*) \rangle \sim (\mu_Q - \mu_*)^{1/2}$. This can be succinctly encoded in a simple mean-field free energy, $F(\varphi) = \frac{1}{2}c_2(T - T_c(\mu_Q))\varphi^2 + \frac{1}{4}c_4(\mu_* - \mu_Q)\varphi^4 + \frac{1}{6}c_6\varphi^6$, with $\varphi \sim \langle \mathcal{O} \rangle$ and with coefficients $c_2, c_4, c_6 > 0$.

3.4. Setting $\mu_Q = 0$ and the persistence of condensates

Fundamental to our construction is that the scalar operator carries a charge q under a global symmetry of the boundary theory. μ_Q tells us the energy cost for adding a unit of this charge to the system. In AdS, superfluid condensation is often induced by tuning μ_Q beyond a threshold. Is this also necessary in the NR case?

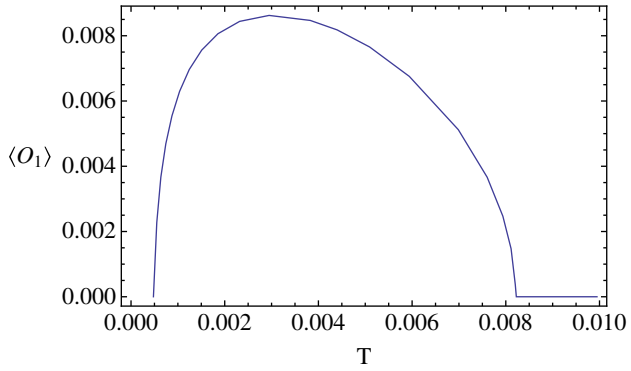

Figure 9. The condensate as a function of T for $\mu_Q = 0$ and $\Omega = 1/16$.

Figure 9 plots the condensate at $\mu_Q = 0$ as a function of T, revealing that condensation persists even without turning on a chemical potential for the global charge. The form of this curve is similar to the large-Ω case studied above with $\mu_Q \neq 0$, modulo an overall scaling of the condensate. It is tempting to speculate that this indicates two distinct pairing mechanisms, one involving the charge and one involving the mass eigenvalue alone. It would be interesting to explore this point further.

4. Conclusions and open questions

In this paper, we have constructed a toy model of superfluid states in holographic NRCFTs and studied the resulting phase diagram, thus finding several unanticipated features. Firstly, as we lower the temperature in the disordered metallic state, the system generally undergoes a phase transition to a superfluid state. At small (and even vanishing) chemical potential, this transition is second order with mean-field exponents; at large chemical potential, however, the transition runs strongly first order. Secondly, for large background mass density, the superfluid state only appears in a finite temperature window, with the metallic state re-entering at sufficiently low temperature. Finally, at zero temperature, the re-entrance of the metallic phase leads to an apparent quantum phase transition from superconducting to metallic as the background mass density is varied.

Several features of our results deserve further scrutiny. Firstly, our low-temperature results derive from a probe analysis which is not valid at zero temperature—indeed, as we push the temperature to zero near or below the putative quantum phase transition at Ω_*, the bulk profiles of various fields grow rapidly, diverging as we approach zero temperature. To be sure, we checked the consistency of the probe approximation in each calculation presented above. However, it is entirely possible that several of our results could change qualitatively when we include backreaction. To nail down the $T = 0$ physics, we must incorporate backreaction.

We have tacitly assumed that the neutral black-hole geometry is the dominant saddle at $T = 0$. However, for a variety of reasons including the strange thermodynamics of this black hole, this seems unlikely to be the case. It is tempting to speculate that the low-temperature phase is dominated by a Schrödinger soliton analogous to the AdS soliton that dominates the relativistic case à la Hawking–Page [4, 23]. Indeed, such a simple Schrödinger soliton solution is

known, and we repeat the above analysis for this geometry in an appendix. However, the black hole and the soliton enjoy incommensurate asymptotic periodicity conditions, so they cannot contribute to the same ensembles. Understanding the true low-temperature ground state of the neutral black hole, even in the absence of any charge density in the system, is of considerable interest.

To this end, it is worth emphasizing that the basic trouble with the thermodynamics of this—and indeed all known—asymptotically Schrödinger black holes is the light-cone relation between the near-horizon killing vector ∂_τ and the asymptotic time-like killing vector, ∂_t. In most constructions, this follows from the structure of the salient solution-generating technique. The challenge, then, is to build solutions that do not flow to AdS black holes near the horizon.

Meanwhile, it is important to keep in mind that the simple Abelian–Higgs theory we study is an extremely stripped down toy model for which we do not have an explicit charged black-hole solution. In the few examples where such a solution is known [16, 17], the matter sectors are considerably more complicated, which is why we worked with the toy model at hand as a first step. It would be interesting to repeat our analysis in one of these more elaborate systems to disentangle the peculiarities of our toy model from general features of NR holographic superfluids.

Finally, several intriguing features of this system still need to be interpreted. Why does the standard quantization have a thermodynamically dominant high-temperature instability, what does that instability signal and is there a simple low-energy way of seeing that this quantization is disfavored? Our conductivity calculations reveal a number of quasiparticle peaks with rather peculiar behavior, particularly near the critical point at Ω_*—are these artifacts of the probe approximation or do they signal real physics, and if so, what are they telling us? Does a proper holographic renormalization of the full system (which remains an open problem) alter any of our results, and if so, how? What about the pairing mechanism—what is the fermion spectral function in these systems and can we correlate pairing of probe fermions with the condensation seen above? We hope to return to some of these questions in future work.

Acknowledgments

We thank K Balasubramanian, O DeWolfe, N Iqbal, S Kachru, P A Lee, H Liu, R Mahajan, J McGreevy, Y Nishida, K Rajagopal and D Vegh for valuable discussions. AA thanks the Aspen Center for Physics and the Stanford Institute for Theoretical Physics, and JW thanks Simons Center for Geometry and Physics at Stony Brook for hospitality during the final stages of this work. The work of AA was supported in part by funds provided by the US Department of Energy (DOE) under cooperative research agreement DE-FG0205ER41360.

Appendix A. Superfluids in a Schrödinger soliton

It is interesting to apply the approach developed above to a slightly different geometry, the so-called Schrödinger soliton [15],

$$ds^2_{\text{soliton,Str}} = \left(-f_s + \frac{(f_s-1)^2}{4(K_s-1)}\right)\frac{dt^2}{K_s r^4} + \frac{1+f_s}{r^2 K_s} dt\, d\xi + \frac{K_s-1}{K_s} d\xi^2 + \frac{d\vec{x}^2}{r^2} + \frac{dr^2}{f_s r^2}, \tag{A.1}$$

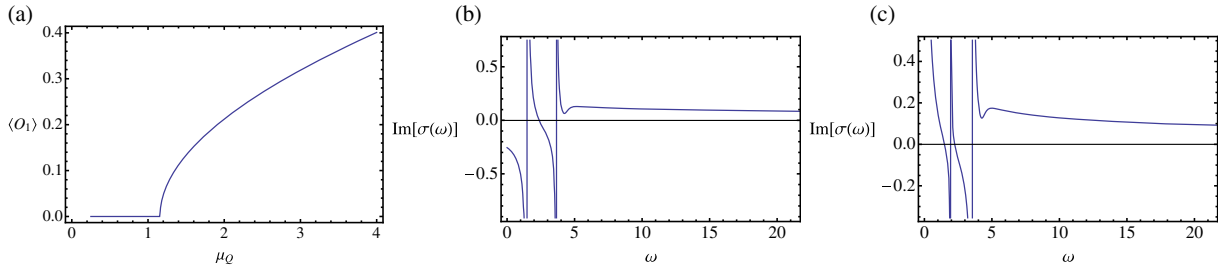

Figure A.1. (a) We found a second-order phase transition at $\mu_c = 1.17$. (b) When $\mu_Q < \mu_c$, $\mathrm{Im}[\sigma(\omega \to 0)]$ is finite, indicating an insulating phase. (c) For $\mu_Q > \mu_c$, we found a superconducting $\frac{1}{\omega}$ pole, as well as two gapped poles at finite ω.

where $K_s = 1 - r^2\Omega^2$ and $f_s = 1 - r^4/r_s^4$, with r_s controlling both the gap and the radius of the ξ-direction, $L_\xi = \frac{\pi}{\Omega r_s}$. Here, the radial direction is cut off smoothly by a spacelike circle shrinking rather than by a black-hole horizon—and indeed this solution was obtained by double Wick rotating the Schrödinger black hole with the compact ξ-direction (which is spacelike near the horizon).[7]

As in the black-hole case, a probe superfluid in the soliton geometry is characterized by five parameters: two define the theory (the dimension Δ and mass M), two are properties of the background which fix thermodynamic quantities (the mass density Ω and mass gap of the soliton, $m_G = \frac{1}{L_\xi}$) and, finally, the $U(1)$-charge chemical potential μ_Q determined by the non-normalizable mode of the bulk gauge field A_t. In the remainder of this appendix, we briefly summarize the results.

A.1. Varying μ_Q

Figure A.1(a) shows the condensate as a function of the chemical potential μ_Q, revealing a critical minimum value μ_c at which the system undergoes a second-order transition with mean-field exponent. For $\mu_Q < \mu_c$, $\mathrm{Im}[\sigma(\omega \to 0)] \to$ finite, indicating a translationally invariant insulating phase. For $\mu_Q > \mu_c$, by contrast, $\mathrm{Im}[\sigma(\omega \to 0)] \sim \frac{1}{\omega}$, indicating superconductivity. We would thus find a second-order insulator–superconductor quantum phase transition by varying μ_Q. However, in addition to this $\omega \to 0$ pole, we found two more mysterious poles at ω_1 and ω_2 separated by a finite gap. This is reminiscent of the paired poles we found in the black-hole system at intermediate values of the background density near the critical point at Ω_*. This transition also recalls the AdS transitions studied in [24].

[7] It is tempting to identify this solution as a low-temperature confined phase of the Schrödinger black hole studied above, analogous to the Hawking–Page transition from the AdS black hole to AdS soliton [4, 23]. However, this is not correct: regularity of the Euclidean solutions imposes incompatible periodicity conditions. More precisely, for the black hole, smoothness of the global Euclidean geometry and compactness of the direction dual to the mass operator require the periodicities $it_b \equiv it_b + n/T$ and $\xi_b \equiv \xi_b + n\mu_Q/T + wL_\xi$. For the soliton, on the other hand, we need $it_s \equiv it_s - in/T_s$ and $\xi_s \equiv \xi_s + in\mu_Q/T_s + wL_\xi$. The inequivalence of these conditions (note, in particular, the extra factor of i in T_s) tells us that these solutions correspond to inequivalent ensembles.

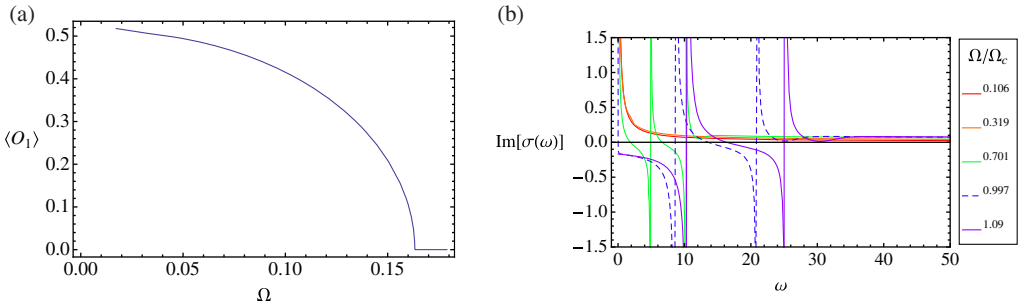

Figure A.2. (a) A second-order superfluid–insulator quantum phase transition at $\Omega_c = 0.163$. (b) For $\Omega > \Omega_c$, we found an insulating gap. For $\frac{1}{2}\Omega_c < \Omega < \Omega_c$, we found a superconducting pole, plus two isolated poles. For $\Omega < \frac{1}{2}\Omega_c$, these poles merge with the zero-frequency superconducting pole.

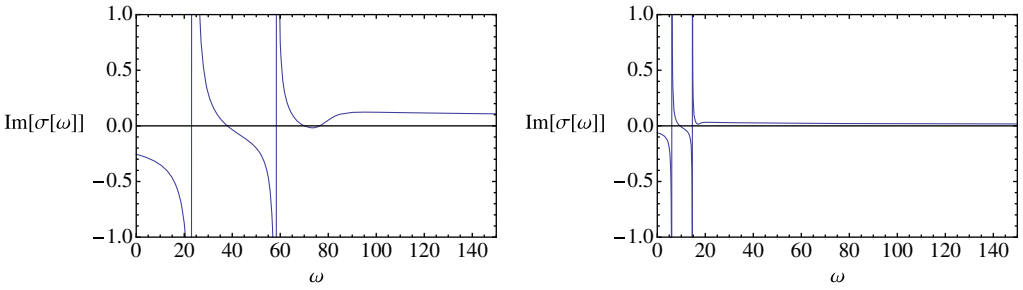

Figure A.3. Varying m_G rescales the insulating gap. Here, $m_G = \frac{1}{4\pi}$ (left) and $\frac{1}{16\pi}$ (right).

A.2. Varying Ω

In the black-hole case, tuning Ω drove us through a superfluid–conductor phase transition at zero temperature. The (zero-temperature) soliton shows the same effect, with the spontaneous condensate disappearing in a second-order transition as Ω passes through a critical value, $\Omega_c \sim 0.163$, as shown in figure A.2(a). Here, however, the normal phase is an insulator (cf figure A.2(b)) with the gap controlled by $(\Omega - \Omega_c)$ and a double-pole structure as seen above. Interestingly, this double-pole structure persists into the superconducting phase, with the gapped poles merging with the zero-frequency poles at a finite value of $\Omega \sim \frac{1}{2}\Omega_c$.

A.3. Varying m_G and the gap

In the above, we have fixed m_G. As it turns out, the only effect of varying m_G is to rescale the gaps in all the above (see figure A.3). This fits nicely with naive intuition for the effect of the compactification radius of the ξ-direction.

Appendix B. Scaling symmetries

The system described by (2.1) and (2.2) enjoys three distinct scaling symmetries, which we can use to fix various parameters to convenient values. Re-introducing G_N and R_A in the action and

metric, the three scaling symmetries act as

Scaling symmetry	t	ξ	x_i	r	T	Ω	$r_{\rm H}$	ds^2	ϕ	A_t	A_ξ	G_N	q	m
α_1	0	0	0	0	0	0	0	-4	0	-2	-2	0	2	2
α_2	0	0	0	0	0	0	0	0	-2	-2	-2	4	2	0
α_3	-2	0	-1	-1	2	1	-1	0	0	2	0	0	0	0

(B.1)

The first two symmetries can be used to fix $\frac{1}{16\pi G_N} = 1$ and $R_A = 1$. The third, which is the basic scaling symmetry of the Schrödinger system with dynamical exponent $z = 2$, can be used to fix $r_{\rm H}$ to a convenient reference value, r_0. Given that $T = \frac{1}{\pi \Omega r_{\rm H}^3}$, this fixes a relation between T and Ω. To access more general values of these parameters, corresponding to $(r'_{\rm H}, T', \Omega')$, we simply map the system to $(r_0, T, \Omega) = (\lambda^{-1} r'_{\rm H}, \lambda^2 T', \lambda^1 \Omega')$, with all physical parameters correspondingly rescaled. (As usual, taking $q \to \infty$ while fixing $q\Phi$ for each matter field Φ gives us a probe limit in which backreaction is negligible [25].)

References

[1] Giorgini S, Pitaevskii L P and Stringari S 2008 *Rev. Mod. Phys.* **80** 1215 (arXiv:0706.3360)
Bloch I, Dalibard J and Zwerger W 2008 *Rev. Mod. Phys.* **80** 885 (arXiv:0704.3011)
Ketterle W and Zwierlein M W 2008 *Proc. Int. School of Physics 'Enrico Fermi'* ed M Inguscio, W Ketterle and C Salomon (Amsterdam: IOS Press) pp 247–422 (arXiv:0801.2500)

[2] Maldacena J M 1998 *Adv. Theor. Math. Phys.* **2** 231
Maldacena J M 1999 *Int. J. Theor. Phys.* **38** 1113 (arXiv:hep-th/9711200)

[3] Gubser S S, Klebanov I R and Polyakov A M 1998 *Phys. Lett.* B **428** 105 (arXiv:hep-th/9802109)

[4] Witten E 1998 *Adv. Theor. Math. Phys.* **2** 253 (arXiv:hep-th/9802150)

[5] Mehen T, Stewart I W and Wise M B 2000 *Phys. Lett.* B **474** 145 (arXiv:hep-th/9910025)

[6] Nishida Y and Son D T 2007 *Phys. Rev.* D **76** 086004 (arXiv:0706.3746)

[7] Son D T 2008 *Phys. Rev.* D **78** 046003 (arXiv:0804.3972)

[8] Balasubramanian K and McGreevy J 2008 *Phys. Rev. Lett.* **101** 061601 (arXiv:0804.4053)

[9] Adams A, Balasubramanian K and McGreevy J 2008 *J. High Energy Phys.* JHEP0811(2008)059 (arXiv:0807.1111)

[10] Herzog C P, Rangamani M and Ross S F 2008 *J. High Energy Phys.* JHEP0811(2008)080 (arXiv:0807.1099)

[11] Maldacena J, Martelli D and Tachikawa Y 2008 *J. High Energy Phys.* JHEP0810(2008)072 (arXiv:0807.1100)

[12] Gubser S S 2008 *Phys. Rev.* D **78** 065034 (arXiv:0801.2977)

[13] Hartnoll S A, Herzog C P and Horowitz G T 2008 *Phys. Rev. Lett.* **101** 031601 (arXiv:0803.3295)

[14] Guica M, Skenderis K, Taylor M and van Rees B 2010 arXiv:1008.1991

[15] Mann R B 2010 *Phys. Lett.* B **686** 188–91 (arXiv:0903.4228)

[16] Adams A, Brown C M, DeWolfe O and Rosen C 2009 *Phys. Rev.* D **80** 125018 (arXiv:0907.1920)

[17] Imeroni E and Sinha A 2009 *J. High Energy Phys.* JHEP0909(2009)096 (arXiv:0907.1892)

[18] Klebanov I R and Witten E 1999 *Nucl. Phys.* B **556** 89 (arXiv:hep-th/9905104)

[19] Cremonesi S, Melnikov D and Oz Y 2010 *J. High Energy Phys.* JHEP1004(2010)048 (arXiv:0911.3806)

[20] Iqbal N, Liu H, Mezei M and Si Q 2010 *Phys. Rev.* D **82** 045002 (arXiv:1003.0010)
Iqbal N, Liu H, Mahajan R and Mezei M to appear

[21] Ross S F and Saremi O 2009 *J. High Energy Phys.* JHEP0909(2009)009 (arXiv:0907.1846)

[22] Marolf D and Ross S F 2006 *J. High Energy Phys.* JHEP0611(2006)085 (arXiv:hep-th/0606113)
[23] Hawking S W and Page D N 1983 *Commun. Math. Phys.* **87** 577
[24] Nishioka T, Ryu S and Takayanagi T 2010 *J. High Energy Phys.* JHEP1003(2010)131 (arXiv:0911.0962)
[25] Hartnoll S A, Herzog C P and Horowitz G T 2008 *J. High Energy Phys.* JHEP0812(2008)015 (arXiv:0810.1563)